3
Models of Gemini Surfactants

HAIM DIAMANT and DAVID ANDELMAN Tel Aviv University, Tel Aviv, Israel

I. INTRODUCTION

Gemini surfactants are composed of two monomeric surfactant molecules linked by a spacer chain. They constitute a new class of amphiphilic molecules having its own distinct behavior. Since their first systematic studies over a decade ago, gemini surfactants have been the subject of intensive research (see Ref. 1 and references therein). Research has been motivated by the advantages of gemini surfactants over regular ones with respect to various applications [e.g., their increased surface activity, lower critical micelle concentration (cmc), and useful viscoelastic properties such as effective thickening].

In addition to their importance for applications, the behavior of gemini surfactants is qualitatively different in several respects from that of regular surfactants, posing challenges to current theories of surfactant self-assembly. The main puzzles raised by gemini surfactants can be summarized as follows [1]:

- *Surface behavior*. The area per molecule in a saturated monolayer at the water–air interface, made of gemini surfactants with polymethylene spacers (*m-s-m* surfactants, where *s* is the spacer length and *m* the tail length in hydrocarbon groups), has a nonmonotonous dependence on *s* [2,3]. For example, for a tail length of $m = 12$, the molecular area at the water–air interface is found to increase with *s* for short spacers, reach a maximum at about $s \simeq 10$–12, and then decrease for longer spacers. This decrease in the specific area for the *m-s-m* surfactants is somewhat unexpected given the fact that the molecule becomes larger as *s* increases. One would naively expect a monotonous increase in the molecular area as, indeed, is observed for another class of gemini surfactants having a poly(ethylene oxide) spacer (m-EO_x-m surfactants) [4,5].

- *Micellization point*. The cmc of gemini surfactants is typically one to two orders of magnitude lower than that of the corresponding monomeric surfactants having the same head and tail groups [6]. For regular (monomeric) surfactants, the cmc decreases monotonously with the number of hydrocarbon groups because of increased molecular hydrophobicity. In the case of *m-s-m* gemini surfactants, by contrast, the dependence of the cmc on the spacer length s is nonmonotonous with a maximum at about $s \simeq 4$–6 [6–8]. Similarly, the Krafft temperature exhibits a minimum [9] and the micellization enthalpy exhibits a maximum [10] at about the same s value.
- *Aggregate Shape*. As certain parameters, such as the relative size of the head and tail groups or the salt concentration, are progressively changed, regular surfactants change their aggregate morphology in the direction of decreasing curvature (e.g., from spherical micelles to cylindrical micelles to bilayer vesicles) [11,12]. However, when the polymethylene spacer length in *m-s-m* gemini surfactants is increased, a different sequence of shape is observed—for instance, from cylindrical micelles to spherical micelles to vesicles for the 12-*s*-12 surfactants [13,14]. Moreover, gemini surfactants with short spacers exhibit uncommon aggregate morphologies in the form of branched cylindrical micelles and ring micelles [15].
- *Phase behavior*. The spacer length in *m-s-m* gemini surfactants has an unusual effect also on the phase behavior of binary surfactant–water mixtures. For geminis with tail length $m = 12$, for instance, the phase-diagram region corresponding to hexagonal and lamellar phases is found to shrink with increasing s, disappear for $s = 10$–12, and reappear for $s = 16$ [16]. In ternary systems containing water, oil, and *m–s–m* surfactant, the size of the microemulsion (single-phase) region in the phase diagram has a nonmonotonous dependence on s with a maximum at $s \simeq 10$ [17].
- *Dynamics*. Dilute micellar solutions of gemini surfactants with short spacers have unusual rheological properties, such as pronounced increase in viscosity upon increase of surfactant volume fraction [18,19] and shear thickening [20,21].

In view of the amount of experimental work and its unusual findings, the number of theoretical studies devoted to gemini surfactants has been surprisingly small. In this chapter, we have, therefore, two aims. The first is to review the current state of theoretical models of gemini surfactants. The second, perhaps more important aim, is to indicate the considerable gaps in our knowledge and the key open questions awaiting theoretical work. In Section II, we set the stage by reviewing several theoretical models of surfactant self-assembly. This will facilitate the discussion in Section III of the gemini surfactant models, which can be viewed as extensions to previous models of

regular surfactants. Finally, in Section IV, we conclude and summarize the open questions.

II. MODELS OF SURFACTANT SELF-ASSEMBLY

In this section, we review several theoretical models pertaining to the self-assembly of soluble surfactants. This is not meant to be an exhaustive review of self-assembly theory but merely to provide the appropriate background for the models of gemini surfactants discussed in Section III.

A. Surface Behavior

Let us start by considering an aqueous surfactant solution below the cmc. The soluble surfactant molecules self-assemble into a condensed layer at the water–air interface, referred to as a Gibbs monolayer (to be distinguished from a Langmuir monolayer that forms when insoluble surfactants are spread on the water–air interface) [22]. Because the surfactant is water soluble, this layer exchanges molecules with the bulk solution and a nonuniform concentration profile forms. Typical surfactants have strong surface activity (i.e., the energy gained by a molecule when it migrates to the surface is much larger than the thermal energy $k_B T$). As a result, the concentration profile drops sharply to its bulk value within a molecular distance from the surface (hence the term *monolayer*).

The number of molecules participating in a Gibbs monolayer per unit area, the surface excess Γ, is obtained by integrating the excess concentration (with respect to the bulk one) over the entire solution. Such a monolayer can be regarded as a separate subsystem at thermodynamic equilibrium and in contact with a large reservoir of molecules having temperature T and chemical potential μ. From the excess free energy per unit area of this system, $\gamma(T, \mu)$, which is by definition the surface tension of the solution, we get the number of molecules per unit area:

$$\Gamma = -\left(\frac{\partial \gamma}{\partial \mu}\right)_T \tag{1}$$

This is referred to as the Gibbs equation [22]. For dilute solutions $\mu \propto k_B T \ln C$, where C is the bulk surfactant concentration. (The constant of proportionality is 1 for nonionic surfactants and ionic surfactants at a high salt concentration; it has a higher value for salt-free ionic surfactant solutions, where strong correlations between the different ions lead to nonideal activity coefficients [22].) Hence,

$$\Gamma \propto -\frac{1}{k_B T}\left(\frac{\partial \gamma}{\partial \ln C}\right)_T \tag{2}$$

Because of the high surface activity of surfactant molecules, leading to a sharp concentration profile at the water–air interface, Γ^{-1} is commonly interpreted as the average surface area per molecule, a. The second consequence of the high surface activity is that, already for C much smaller than the cmc, the monolayer becomes saturated (i.e., Γ stops increasing with C). Experimentally, the curve describing the change in γ as a function of ln C becomes a straight line with a negative slope proportional to $-\Gamma$.

We now wish to find a simple estimate for the energy of lateral interaction between molecules in such a saturated monolayer (repeating a well-known result of Ref. 11). Saturation implies that the molecules are packed in an energetically optimal density, such that there is no gain in adding or removing molecules. This optimum arises from a competition between attractive and repulsive interactions. The attractive interaction tries to decrease the area per molecule, and we can phenomenologically write its energy per molecule as proportional to a, $\gamma_1 a$, where the proportionality constant γ_1 has units of energy per unit area. Because the attraction comes mainly from the desire of the hydrocarbon tails to minimize their contact with water, γ_1 should be roughly equal to the hydrocarbon–water interfacial tension ($\gamma_1 \simeq 50$ mN/m). The repulsive interaction, on the other hand, tries to increase a and, at the same phenomenological level, we can write its energy per molecule as inversely proportional to a, α/a, where α is a positive constant. Minimizing the sum of these two contributions, we get for the interaction energy per molecule $u = \gamma_1(a-a_0)^2/a + \text{const}$, where $a_0 = (\alpha/\gamma_1)^{1/2}$ is the optimal molecular area. Expanding around $a = a_0$ to second order and omitting the constant term, we obtain

$$u(a) \simeq \frac{\gamma_1}{a_0}(a - a_0)^2 \tag{3}$$

This is merely a harmonic approximation for the interaction energy associated with small deviations from optimal packing.

We can slightly modify this result to obtain a similar harmonic estimate for the energy u_2 of effective interaction between *two* neighboring molecules residing in the saturated monolayer. (This will be useful later when we add the spacer to form gemini surfactants.) We need to divide u by half the number of in-plane neighbors, $q/2$, and express a in terms of the average intermolecular distance r, $a = \eta r^2$, where η is a prefactor of order unity (e.g., for hexagonal packing $q = 6$ and $\eta = \sqrt{3}/2 \simeq 0.9$). Assuming, again, that r is close to its optimal value r_0, we get

$$u_2(r) \simeq \frac{1}{2}k_0(r - r_0)^2, \qquad k_0 = \frac{16\eta\gamma_1}{q} \tag{4}$$

This expression replaces the actual surfactant–surfactant interaction in the monolayer, including effects of other nearby surfactants, with an effective spring of equilibrium length r_0 and spring constant k_0. For hexagonal packing, we get the reasonable value $k_0 \simeq 120$ mN/m $\simeq 0.3 k_B T/\text{Å}^2$. Note that, because of the saturation condition, the expression for k_0 is insensitive to molecular details. In turn, those details will affect the properties of the saturation state itself (e.g., the value of a_0 or r_0).

B. Micelles

As the solution concentration is increased beyond the cmc, the surfactant molecules start to form aggregates. Unlike simple solute molecules (e.g., alkanes), which undergo macroscopic phase separation upon increasing concentration or changing temperature, surfactants form micelles at the mesoscopic scale. The challenges posed to theories of surfactant self-assembly are to predict the micellization point as a function of concentration (i.e., the cmc, hereafter referred to by the corresponding volume fraction φ_{cmc}) and temperature (T_m), as well as the micelle shape and size. The main complications come from the fact that micellization is *not* a macroscopic phase transition—the aggregate sizes are finite and polydisperse—and, thus, the well-developed theoretical framework of phase transitions does not strictly apply.

From a thermodynamic point of view, the difference between surfactant micellization and phase separation lies in the following observation [12]. For alkanes solubilized in water, for example, the (Gibbs) free energy per molecule in an aggregate of size N, g_N, is a monotonously decreasing function of N—for $N \to \infty$, g_N tends to the free energy per molecule in the bulk alkane phase, g_∞, whereas for smaller N, $g_N > g_\infty$ due to unfavorable surface terms of the finite cluster. As a result, there is a critical concentration (or critical temperature) at which the favorable size changes discontinuously from monomers solubilized in water ($N = 1$) to a macroscopic phase of bulk alkane ($N \to \infty$). The first-order phase transition point is reached when the chemical potential of monomers exceeds $\min\{g_N\} = g_\infty$. In a dilute solution, this implies that $\varphi_c = \exp[g_\infty/(k_B T)]$, $k_B T_c = g_\infty/\ln \varphi$. (We have set the free energy of the $N = 1$ state as the reference, $g_1 = 0$.) In the case of surfactants, by contrast, g_N has a minimum at a finite aggregate size N^*. As a result, when the chemical potential exceeds g_{N^*}, a large population of aggregates appears, whose sizes are distributed around N^*. Hence, the micellization point can be estimated as

$$\varphi_{\text{cmc}} = \exp^{g_{N^*}/k_B T}, \quad k_B T_m = \frac{g_{N^*}}{\ln \varphi} \tag{5}$$

The remaining task is to obtain a theoretical expression for $g_N^{(s)}$, the free energy per molecule in aggregates of size N and shape S. Because we expect

this function to have a minimum at a finite yet large N (say, $N^* \sim 10^2$), the importance of many-body interactions is inevitable, and obtaining $g_N^{(s)}$ from rigorous statistical mechanics is a formidable task. Consequently, analytical models have relied on phenomenological approaches, trying to account for various competing contributions to the free energy while assuming a certain geometry for the aggregate [11,12,23]. From the minimum of $g_N^{(s)}$ with respect to N and various possible shapes S, one can obtain the aggregate shape, aggregation number, and micellization point, using Eq. (5).

In the simplest picture [11,12], rough estimates for the minimum of $g_N^{(s)}$ can be obtained by imposing geometrical constraints that arise from the incompressibility of the micellar hydrocarbon core (see Fig. 1). These constraints lead to a finite aggregation number N^*, as required. The hydrocarbon tail chains cannot extend beyond a certain length l, and each tail must occupy a certain volume v. (Both l and v are known to have a simple linear dependence on the number of hydrocarbon groups in the tail chain [24].) In addition, as in the case of the Gibbs monolayer of Section II.A, surfactant molecules in the favorable aggregate state attain a certain optimal area per molecule a_0. Then, due to translational entropy, the favorable aggregates would be the smallest

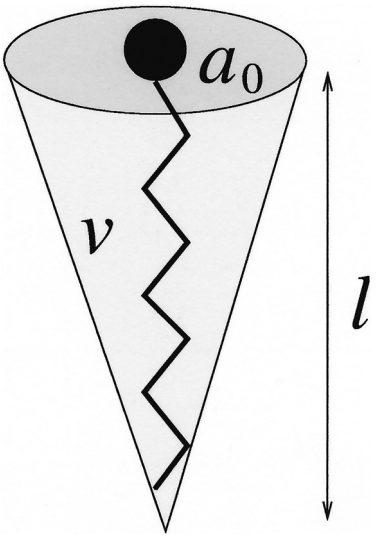

FIG. 1 Packing constraints on a surfactant in an aggregate. Each head group occupies an optimal area a_0 on the aggregate surface; the tail chain occupies a volume v and cannot stretch beyond length l. These constraints define the packing parameter, $P = v/a_0 l$, which suggests the possible aggregate shape.

ones that satisfy all constraints. The constraints define a dimensionless packing parameter (Fig. 1),

$$P = \frac{v}{a_0 l} \tag{6}$$

If $P <$ one/third, the constraints can be satisfied by spherical micelles, which will be the smallest and hence the most favorable ones; when $\frac{1}{3} < P < \frac{1}{2}$, the micelles will have to be of elongated or cylindrical shapes; for $\frac{1}{2} < P < 1$, planar shapes will form; and for $P > 1$, the morphology must be inverted.

Once the shape is determined, we can find the maximum allowed aggregation number. For example, for spherical micelles $N < 4\pi l^2/a_0 = (4\pi/3)l^3/v$, and we get

$$N < 36\pi \frac{v^2}{a_0^3} \tag{7}$$

We see how competing interactions between the molecules (giving rise to a_0) together with the incompressibility of the micellar core lead to finite micelles. Because the tail chains usually should not stretch to their full extent, the actual aggregation number will be smaller than this upper bound.

Yet, these geometrical arguments cannot provide us with theoretical predictions as to the optimal molecular area a_0 itself or the aggregation free energy $g_N^{(s)}$, as well as their dependence on parameters such as temperature or salt concentration. In order to get such information and subsequently predict the micellization point, micelle shape, and size, one needs a more detailed theory.

1. Phenomenological Models

There have been attempts to analytically account for the various competing contributions to the free energy per molecule $g_N^{(s)}$ (e.g., Ref. 23). The advantage of this approach is that once we have an expression for the free energy, we can easily change parameters and gain insight into the role of various contributions. On the other hand, such models essentially attempt to push the limits of the phenomenological approach toward a detailed molecular description. They usually entail uncontrolled approximations and parameters whose accurate values are often hard to obtain. As an example, which will serve us in Section III, we give an analysis along the lines of (yet not identical to) Ref. 23.

Five major contributions to the aggregation free energy (per surfactant molecule on the aggregate) can be considered [23]:

$$g_N^{(s)}(a) = g_{hc} + g_{int}(a) + g_{es}(a, R) + g_{st}(a) + g_{el}(R) \tag{8}$$

where a is the area per molecule on the aggregate surface and R is the aggregate size (radius or width). Note that R is not an independent variable but is related to N and a via the aggregate geometry S (e.g., for spherical micelles, $Na = 4\pi R^2$). The five contributions are as follows:

1. The driving force for aggregation is the hydrophobic effect (i.e., the free energy per surfactant molecule g_{hc} gained by shielding the hydrocarbon groups from water) [24]. This contribution to $g_N^{(s)}$ is negative and, to a good approximation, independent of N and the aggregate geometry S; namely its contribution to the *entire* aggregate free energy is linear in N and tends to increase the aggregate size. The hydrophobic term g_{hc} depends linearly on the number of hydrocarbon groups in the surfactant, with a reduction of roughly k_BT per hydrocarbon group [12]. That is why, for regular surfactants, the cmc decreases exponentially with the number of hydrocarbon groups in the molecule and is reduced by a factor of roughly 2–3 per each additional hydrocarbon group.
2. The hydrophobic gain is corrected by an interfacial contribution g_{int} due to the unfavorable contact between the hydrocarbon core and water:

$$g_{\text{int}}(a) = \gamma_1(a - a_{\min}) \tag{9}$$

   where γ_1 is the interfacial tension of the core–water interface (roughly equal to the hydrocarbon–water interfacial tension) and $a_{\min}$ is the minimum area per molecule (i.e., the interfacial area occupied by a head group). This contribution evidently acts to reduce the area per molecule.
3. If the surfactant head groups are charged, there is electrostatic repulsion between them, acting to increase a. Within the Poisson–Boltzmann theory, this electrostatic contribution is given by [25]

$$g_{\text{es}} = \frac{2k_BT}{\beta}\left\{\beta \ln\left[\beta + \left(1+\beta^2\right)^{1/2}\right] - \left(1+\beta^2\right)^{1/2} + 1 - 2c\lambda_D \ln\left[\frac{1}{2} + \frac{1}{2}(1+\beta^2)^{1/2}\right]\right\}, \tag{10}$$

   where $\beta = 4\pi l_B \lambda_D / a$ is a dimensionless charging parameter depending on two other lengths: the Debye screening length λ_D and the Bjerrum length l_B. The Debye screening length in the solution is $\lambda_D = (8\pi l_B C_{\text{salt}})^{-1/2}$, where C_{salt} is the added salt concentration, taken here to be monovalent, and $l_B = e^2/\varepsilon k_B T$ is about 7 Å for aqueous solution with dielectric constant $\varepsilon = 80$ at room temperature. (For simplicity, a monovalent head group has been assumed.) Finally, c is the mean curvature of the aggregate (e.g., $1/R$ for spherical micelles).

4. There is also steric repulsion between head groups. From the (nonideal) entropy of mixing per molecule, for this contribution we get

$$g_{\mathrm{st}}(a) = k_B T\left[\ln\left(\frac{a_{\min}}{a}\right) + \left(\frac{a}{a_{\min}} - 1\right)\ln\left(1 - \frac{a_{\min}}{a}\right)\right] \tag{11}$$

5. The last contribution to the free energy is associated with the tail packing in the hydrophobic core; that is, deviations of the hydrocarbon tail chains from their relaxed length l_0,

$$g_{\mathrm{el}}(R) = \frac{1}{2}k'(R - l_0)^2 \tag{12}$$

The elastic constant k' depends on the chain statistics, as well as the packing parameter (i.e., aggregate shape) [23].

The equilibrium aggregation number N and specific area a (and hence also aggregate size R) for a given shape S and surfactant chemical potential μ are then determined by the equations

$$g_N^{(\mathrm{s})}(a) = \mu, \qquad \frac{\partial g_N^{(\mathrm{s})}(a)}{\partial a} = 0 \tag{13}$$

Comparing the minimum value of $g_N^{(\mathrm{s})}$ for various shapes S, one also obtains the equilibrium aggregate morphology. As long as $\mu < k_B T \ln \varphi_{\mathrm{cmc}}$, these equations will have no solution, and the monomeric state ($N = 1$) of single surfactant molecules solubilized in water is the stable one. As the chemical potential increases, we reach the micellization condition given by Eq. (5), where the average micelle size at the cmc, N^*, can be calculated now from the expression of $g_N^{(\mathrm{s})}$ at its minimum.

2. Computer Simulations

Another route to overcome the complexity of treating surfactant micellization is to use computer simulations. This approach can be divided into two categories: statistical-mechanical models using Monte Carlo (MC) simulations and molecular dynamics (MD) simulations.

Following Widom's statistical–mechanical model of microemulsions [26], a host of lattice models was presented for treating surfactant self-assembly (see, e.g., Refs. 27–31). These molecular toy models represent the water molecules and various groups in the surfactant as Ising spins on a discrete lattice. The various interactions between the groups are represented by ferromagnetic or antiferromagnetic couplings between nearest-neighbor spins (see Fig. 2). Evidently, this is a very crude description of surfactant solutions and is not expected to yield quantitative predictions. Another difficulty is attaining thermodynamic equilibrium in simulations of these self-assembling

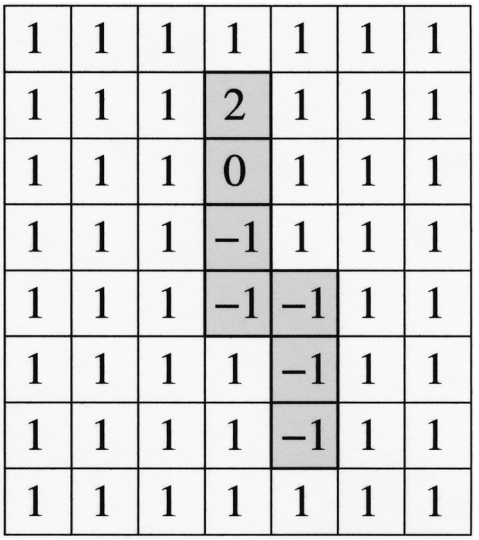

FIG. 2 Schematic representation of a surfactant molecule (gray) solubilized in water (white) in a lattice spin model. Each water molecule and surfactant group are represented by a spin variable on a lattice site. Water molecules have spin $+1$, head groups $+2$, and tail groups -1. In between the head and the tail, there is a neutral group of spin 0. The various particles interact via nearest-neighbor ferromagnetic couplings favoring spins of the same sign, except for the head–head interaction, which is antiferromagnetic, disfavoring neighboring heads. The chain connectivity and the overall number of chains are preserved during the MC simulation.

systems, which contain slowly relaxing, large aggregates. Such models, however, have been shown to correctly reproduce various qualitative features of amphiphilic systems (e.g., aggregate formation, aggregate shape, and the overall structure of phase diagrams). The main advantage of this statistical–mechanical approach is that, by tuning a small number of parameters, from the MC simulations one can get insight into molecular mechanisms that determine the overall system behavior. Here, we briefly present a model similar to that of Ref. 31. It will serve us when we discuss gemini surfactants in Section III.B.

In the lattice model, each water molecule is assigned a spin $\sigma = +1$, a hydrocarbon group in the tail has spin $\sigma = -1$, and the head group has spin $\sigma = +2$ (see Fig. 2). In between the hydrophilic head group and the hydrophobic tail, there is a neutral group of spin $\sigma = 0$. All of the couplings are

ferromagnetic (favoring neighboring spins of the same sign), except for the head–head coupling, which is antiferromagnetic, mimicking head–head repulsion due to screened electrostatics. The energy of the system can be written as

$$E = -J \sum_{\langle ij \rangle} \sigma_i \sigma_j \left(1 - 2\delta_{\sigma_i,2}\delta_{\sigma_j,2}\right) \tag{14}$$

where $J > 0$ is the coupling strength, $\langle ij \rangle$ denotes summation only over nearest-neighbor pairs of the lattice, and $\delta_{i,j} = 1$ when $i = j$ and zero when $i \neq j$ is the Kronecker delta function. Two neighboring water molecules attract each other with energy $-J$ because, then, $\sigma_i \sigma_j = 1$. The same applies to two tail groups, whereas a water molecule and a tail group repel with energy $+J$. The extra factor of $1 - 2\delta_{\sigma_i 2}\, \delta_{\sigma_i 2}$ in Eq. (14) is unity for all cases except when i and j are two heads with $\sigma = +2$, yielding a repulsion of $+4J$ between two head groups. Finally, a head group and a water molecule attract with energy $-2J$, and a head group and a tail group repel with energy $+2J$. These couplings apply whether the two neighboring lattice sites belong to the same molecule or not. In addition, the groups belonging to the same surfactant molecule are kept linked throughout the simulation. Thus, the essential features of hydrophobicity, hydrophilicity, molecular connectivity, and (screened) electrostatic repulsion are all accounted for using the single parameter J. Other parameters are the length of the tail group and total number of surfactant molecules in the system.

The MC simulation starts from a certain configuration of surfactant molecules in water. At each iteration, the various groups of the surfactants are moved while maintaining the connectivity of the molecules, their total number, and the total number of water molecules (e.g., using a "slithering snake" scheme [31]). The energetic cost of the move is calculated using Eq. (14), and the MC step is accepted or rejected according to a Metropolis criterion, ensuring convergence toward equilibrium.

This simple scheme can reproduce much of the richness of surfactant self-assembly, including the formation of monolayers, micelles, and bilayers, the dependence of the cmc on tail length, transitions between various aggregate shapes, and so forth. On the other hand, such models can merely indicate general trends and not detailed information. For example, the correspondence between the MC spin variable representing subgroups of a surfactant molecule and the actual chemical groups is not well defined and remains ambiguous to some extent.

Another class of numerical studies that have been used to explore surfactant self-assembly are molecular dynamics (MD) simulations. These models range in detail from coarse-grained bead–spring representations of the molecules (e.g., Refs. 32–37) to atomistic descriptions (e.g., Refs. 38–42). The

advantage of the MD approach, as compared to phenomenological theories and spin models, is that the description of the system on the molecular scale is less artificial. The disadvantages are the limited spatial and temporal extent of the simulations, entailing equilibration problems, and sometimes also a large number of required parameters. A typical all-atom MD simulation of an aqueous surfactant system may contain about 100 surfactant molecules along with a few thousands of water molecules, and the dynamics can be run for a few nanoseconds (e.g., Ref. 42). A coarse-grained simulation allows a significant increase of these numbers at the expense of molecular detail (see, e.g., Ref. 37). Here, we outline a coarse-grained approach to surfactant micellization, as presented in Ref. 32, which was later extended to gemini surfactants [36].

The MD model of Ref. 32 contains only two types of particles: waterlike and oilike, where a surfactant molecule is composed of a few waterlike particles (the head group) and a chain of oillike particles (the tail). The particles interact via a truncated Lennard-Jones potential,

$$V(r) = \begin{cases} 4\epsilon\left[\left(\dfrac{d}{r}\right)^{12} - \left(\dfrac{d}{r}\right)^{6}\right], & r \le r_c \\ 0, & r > r_c \end{cases} \tag{15}$$

where r is the interparticle distance, ϵ is the energy parameter of the Lennard-Jones potential, d is its length parameter, and r_c is a cutoff. This potential has a minimum at $r_{\min} = 2^{1/6}d$. Hence, for $r_c \le r_{\min}$, the potential is purely repulsive, which is what is chosen for the oil-water interaction. For $r_c > r_{min}$, the potential contains a short-ranged repulsion followed by an attractive region, which is a suitable choice for the water–water and oil–oil interactions. In addition, the particles constituting a single surfactant molecule are connected by harmonic potentials of equilibrium length d and strong spring constant (much larger than ϵ/d^2), ensuring chain connectivity.

The MD simulation starts from a random distribution of surfactants in water. It then evolves in time according to the classical equations of motion governing the motion of individual particles. The simulations typically contain a few tens of thousands of particles and are run for about 10^5–10^6 time steps [32,33,36,37]. Thanks to the coarse-grained description, this can amount to about 1 μs in real system time [37]. Such a scheme was shown to successfully reproduce the structure of monolayers and micelles of various shapes and to provide some understanding of the dynamics of surfactant self-assembly [32,33]. On the other hand, as in the MC case, the coarse-grained representation prevents a well-defined correspondence between the simulated system and the actual molecules in the experiments.

C. Phase Behavior

Concentrated surfactant solutions and ternary water–oil–surfactant systems exhibit a rich variety of disordered and liquid-crystalline phases [43–45]. Some examples are the lamellar (L_α) phase, sponge (L_3) phase, hexagonal (H_1) phase, and cubic (V_1) phase. All of these phases are based on various packing of surfactant layers: bilayers (in the binary-mixture case) or monolayers (in the ternary case). The lamellar phase is made of stacks of parallel layers, the sponge phase contains a disordered arrangement of multiconnected layers, the hexagonal phase consists of hexagonal arrays of parallel cylinders, and the cubic phase contains spherical layers arranged in a cubic lattice.

Unlike micellization, one deals here with macroscopic bulk phases and their corresponding phase transitions. Hence, the powerful tools of thermodynamics and statistical mechanics are applicable. Consequently, the theory of surfactant phase behavior has reached a more advanced level, particularly in the case of phases with long-ranged order. We will not review these theories here, as most of them have not been used in current models of gemini surfactants, but we will merely mention the various approaches.

Two phenomenological approaches to the phase behavior of surfactant binary and ternary mixtures have been used. The first is based on the Ginzburg–Landau formalism, which has been widely used in statistical physics [43]. It starts with a lattice description of the mixture and derives from it a coarse-grained, continuous expression for the energy (Hamiltonian), which can be studied by statistical–mechanical techniques. The second approach is based on the elastic and thermodynamic properties of the membranes that make the various phases. For a review, see, for example, Ref. 45. In addition to these phenomenological theories, a variety of lattice spin models employing Monte Carlo simulations, as discussed in Section II.B, were originally designed and applied to study surfactant phase behavior [26–31].

III. MODELS OF GEMINI SURFACTANTS

Having provided the necessary background, we now turn to models of gemini surfactants. As will be demonstrated in this section, these models are essentially extensions of surfactant self-assembly theories, which have been reviewed in Section II. The binding of the surfactant molecules into pairs via spacer chains introduces new constraints affecting the molecular arrangement in monolayers, micelles, and mesophases, as well as the thermodynamics of self-assembly.

A. Surface Behavior

As in Section II, we begin by looking at a saturated monolayer, this time made of gemini surfactants, lying at the water–air interface. The gemini nature of the molecules (i.e., the introduction of the spacer) adds considerable complexity to the problem, mainly because it introduces anisotropy and inhomogeneity into the monolayer. A schematic view of the surface covered with dimers is shown in Fig. 3. The dimers may be oriented in various directions, and the distances between two linked monomers (in a dimer) and between two unlinked ones will differ in general.

Nevertheless, we are going to disregard these complications and focus on the simplest question: How does the introduction of a spacer consisting of s groups affect the in-plane distance $r_d(s)$ between two monomers belonging to the same dimer? Although seemingly oversimplified, the answer to this question will give us key insight into the surface behavior of gemini surfactants.

We proceed by reviewing and slightly extending the work presented in Refs. 46 and 47. We have seen in Section II.A that the interaction between surfactants in a saturated monolayer can be roughly approximated by effective springs whose equilibrium length r_0 is determined by the optimum packing at saturation and whose spring constant k_0 is given in Eq. (4). Thus,

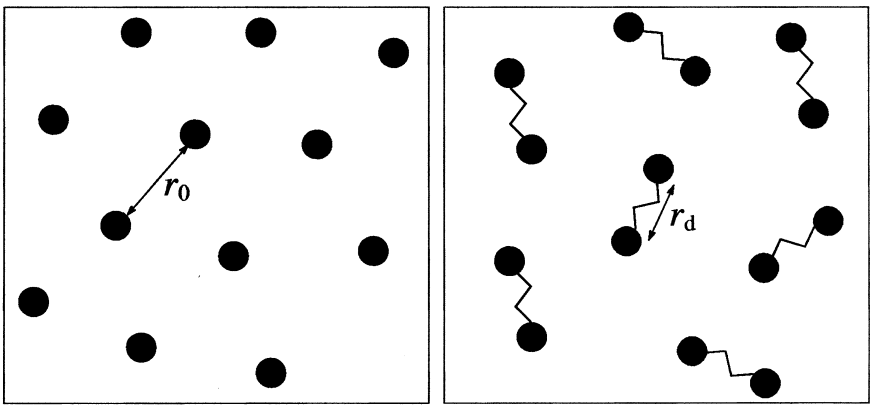

FIG. 3 Schematic top view of a saturated monolayer at the water–air interface. Left: Regular surfactant head groups separated by a mean optimal distance r_0; right: same view of gemini surfactants where the head groups are linked into dimers by spacers. The mean distance between head groups in a dimer is r_d, which, in general, differs from the distance between unlinked head groups.

it is natural to consider the spacer chain as another effective spring, of equilibrium length r_s and spring constant k_s, connecting the two surfactant heads in a dimer. The combination of the two types of monomer–monomer interaction (the one present between unlinked monomers and the one due to the spacer) is then reduced to adding together two springs in parallel. From this, we obtain

$$r_d(s) = \frac{k_0 r_0 + k_s(s) r_s(s)}{k_0 + k_s(s)} \tag{16}$$

The origin of the spacer spring is entropy and its parameters are determined by the statistical distribution of spacer configurations. The equilibrium length of the spring is the mean end-to-end distance of the spacer chain, and the spring constant is inversely proportional to the variance of the end-to-end distance,

$$r_s = \langle r \rangle, \qquad k_s = \frac{k_B T}{\langle r^2 \rangle - \langle r \rangle^2} \tag{17}$$

where the averages are taken over all spacer chain configurations. Thus, the harmonic spring approximation for the spacer is equivalent to representing the actual statistical distribution of spacer configurations by its first two moments.

Before considering specific models for the spacer chain, let us examine what qualitative results are expected from this description. When the spacer is very short and rigid, such that $k_s \gg k_0$, the equilibrium length r_d of the dimer is determined by the spacer, $r_d \simeq r_s$. On the other hand, when the spacer is very long and flexible, such that $k_s \ll k_0$, r_d will be determined by the regular monomer–monomer interaction, $r_d \simeq r_0$. Hence, upon increasing the number s of groups in the spacer, we expect $r_d(s)$ to first increase and then saturate toward r_0, the optimal distance between the monomeric surfactants. Whether the behavior for intermediate spacer lengths is monotonous or not depends on specific details of the spacer chain. If the spacer stiffness $k_s(s)$ drops sufficiently fast with s, the "interaction spring" will start dominating before $r_s(s)$ exceeds r_0, and $r_d(s)$ will then grow monotonously with s. By contrast, if $k_s(s)$ decreases slowly with s, the "spacer spring" will dominate even for quite long spacers and $r_d \simeq r_s$ will become larger than r_0. For even longer s, it will have to *decrease* back toward r_0, leading to nonmonotonous behavior in this case.

The simplest model for the spacer is that of a Gaussian constraint-free chain. This case is somewhat artificial and is discussed here merely as a model for very flexible and long chains, in contrast with more realistic models discussed in the following for more rigid chains. A Gaussian chain consisting

of s segments is analogous to a random walk of s steps. The mean squared displacement of such a walk, averaged over all s-step walks, should scale linearly with s. The mean end-to-end distance of a Gaussian spacer is therefore $r_s \sim bs^{1/2}$, where b is the segment length. More specifically, the statistical distribution of the end-to-end distance in a Gaussian chain is

$$p(r)\,dr = \left(\frac{3}{2\pi s b^2}\right)^{3/2} e^{-3r^2/2sb^2} 4\pi r^2\,dr \tag{18}$$

From the mean and variance of this distribution, we get, according to Eq. (17),

$$r_s(s) = b\left(\frac{8s}{3\pi}\right)^{1/2}, \qquad k_s(s) = \frac{k_B T}{[1 - 8/(3\pi)]b^2 s} \tag{19}$$

Thus, in order to calculate r_s and k_s, we just need to know the segment length b. For a polymethylene spacer, b is 2.53Å. The remaining information required to compute r_d from Eq. (17) are the properties of the *monomeric* surfactant in a saturated monolayer, namely k_0 and r_0. In a roughly hexagonal arrangement of molecules, one has $k_0 \simeq 0.3 k_B T/\text{Å}^2$ (see Section II.A). A saturated monolayer of dodecyltrimethylammonium bromide (DTAB) surfactants, for example, is known to have $a_0 \simeq 55\text{Å}^2$ (i.e., $r_0 \simeq 8$Å). By using these values and substituting Eq. (19) in Eq. (16), r_d as function of s is calculated and depicted as the dashed line in Fig. 4. The intermonomer distance increases moderately with s and even exceeds r_0, yet the maximum and descent back to r_0 are shallow and occur at very large s, lying outside the experimentally relevant range of spacer lengths $1 \leq s \leq 20$ shown in Fig. 4.

More realistically, the spacer chain can be described by the rotational–isomeric model, where each segment in the chain can have only three possible orientations with respect to the two that precede it in the sequence (the three conformations called trans and gauche$^{\pm}$) [48]. In addition, we require that the hydrophobic spacer be restricted to reside in the nonaqueous side of the water–air interface. These constraints stiffen the chain and bias its statistics toward larger end-to-end distances. Therefore, we expect a larger overshoot and a sharper maximum of $r_d(s)$, as is confirmed by the solid curve in Fig. 4. The points of this curve were obtained from simulations of rotational–isomeric polymethylene chains whose ends were fixed to a surface (the air–water interface) and whose segments were forbidden from crossing that surface into the water side (see Ref. 46 for more details). From the simulations, one obtains the end-to-end distance distribution and then extracts the spring parameters r_s and k_s according to Eq. (17) [47].

What has been calculated is the intermonomer distance in a dimer and not the average area per dimer in the monolayer. However, because the latter

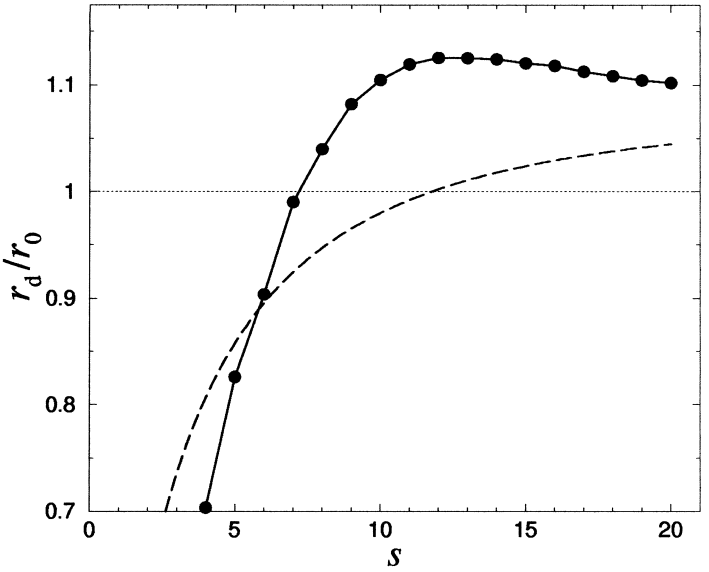

FIG. 4 The distance r_d between the two head groups of a gemini surfactant in a saturated monolayer as a function of the number of groups s in its spacer. The distance is rescaled by r_0, the distance between unlinked heads in a saturated monolayer of the corresponding monomeric surfactant. Curves for two spacer models are shown: Gaussian chain with no constraints (dashed line) and rotational–isomeric chain restricted to the nonaqueous side of the interface (symbols and solid line). The latter has a maximum at $s = 12$, in accord with experimental results of Refs. 2 and 3.

must increase together with the former (cf. Fig. 3), this very simple spring model reproduces the experimental observation of a nonmonotonous behavior of $a(s)$ for the m-s-m gemini surfactants [2] and gemini surfactants derived from arginine [3]. Although the shape of the experimental curve is reproduced only qualitatively, the position of the maximum at $s \simeq 12$ is the same as the one found experimentally for 12-s-12 surfactants [2]. Furthermore, the spring model elucidates the source of the nonmonotonous behavior—a competition between the regular monomer–monomer interactions, on one side, and the natural length and rigidity of the spacer, on the other. According to this picture, we should expect a more moderate and monotonous increase in a for a more flexible spacer chain, as has been demonstrated by the above Gaussian chain example. This may explain the behavior of $a(s)$ observed for the m-EO_x-m gemini surfactants, having more flexible poly(ethylene oxide) spacers [4,5]. (Compare, for example, our Fig. 4 with Fig. 1 of Chapter 4.)

These qualitative features, as well as the maximum at $s \simeq 10$–12, were found to remain unchanged upon various refinements of the model (e.g., the inclusion of nonbonded interactions within the spacer chain or a more detailed treatment of the monolayer structure) [46]. A hydrophobic effect (i.e., repulsion of spacer monomers from the water phase) was invoked in several works as an explanation for a lift off of the spacer from the water surface and hence the maximum in $a(s)$. Such an effect, according to the spring model, actually suppresses the maximum, as it brings the spacer ends closer together and thus reduces the overshoot of r_d. We note that this effect might be related, though, to the maximum observed in the cmc of *m-s-m* surfactants at lower s values; see Section III.B.

The description provided by the spring model is too simplistic to account for various details of gemini surfactant monolayers. In particular, two critical comments can be made. First, the experimentally observed decrease of $a(s)$ for $s > 12$ is much steeper than what the model describes [2]. As has been suggested in Ref. 1, this might be a result of increased premicellar aggregation in the bulk solution as the spacer becomes more hydrophobic. Second, the model regards the spacer as an isolated chain, whereas, in reality, the gemini surfactant has two additional tail chains nearby. In this respect, the model treats the geminis as equivalent to bolaform surfactants. Although undoubtedly the presence of the tails is important for quantitative predictions, it is not expected to alter the above-described qualitative competition picture, and a similar nonmonotonous behavior of $a(s)$ was indeed observed in bolaform surfactants as well [49].

B. Micelles

The micellization behavior of gemini surfactants is qualitatively different from that of regular ones. We have reviewed some of these differences in Section I, and they can now be further elucidated in the light of what we have discussed in the previous sections.

The cmc of gemini surfactants is typically one to two orders of magnitude lower than that of the corresponding monomeric surfactants [6]. The lower cmc can be directly attributed to the increase in the number of hydrocarbon groups in the molecule (i.e., decrease in the hydrophobic contribution g_{hc}) due to the second tail and also due to the hydrophobic spacer chain in the case of *m-s-m* surfactants. Based only on the contribution of a second tail to g_{hc} and the fact that the molecular volume is roughly doubled going from the monomeric surfactant to a gemini one, one would have predicted a *larger* decrease in cmc than what is actually observed. The difference is probably due to unfavorable terms introduced by the spacer, which will be further discussed in this subsection.

The cmc of *m-s-m* gemini surfactants, instead of monotonously decreasing with the number s of spacer hydrocarbon groups (i.e., with molecular hydrophobicity), is a nonmonotonous function with a maximum around $s \simeq 4$–6 [6–8]. A corresponding nonmonotonous behavior is observed in the Krafft temperature [9] and micellization enthalpy [10]. This behavior can be attributed to the straightness and rigidity of short spacers, which force their hydrocarbon groups to be in unfavorable contact with water. At about $s \simeq 4$–6, although the spacer chain is still rigid, a gauche conformation should become accessible, allowing some of the groups to penetrate in the micellar hydrophobic core. When the spacer is hydrophilic, this effect should be absent, as indeed is the case with *m*-EO_x-*m* surfactants, exhibiting a weak monotonous increase of the cmc with the hydrophilic spacer length x [4].

As a function of spacer length s, *m-s-m* surfactants exhibit an unusual progression of aggregate shapes from cylinders to spheres to bilayers. This is different from the more natural succession, occurring in monomeric surfactants, where the change in aggregate curvature is monotonous: spheres transforming into cylinders transforming into bilayers. Assuming that the molecular area at the aggregate surface is related to that in a saturated monolayer, this uncommon behavior can be qualitatively understood in view of the nonmonotonous variation of $a(s)$ as a function of s, as discussed in Section III.A. Considering that the radius and volume of the micellar core depend primarily on the tails and not on the spacers, an increase and then a decrease of a as a function of s should be accompanied by a decrease and then an increase in the packing parameter P of Eq. (6), hence the unusual morphological sequence.

More specific predictions require a detailed theory and will be reviewed next.

1. Phenomenological Model

An extension of the phenomenological theory of surfactant aggregation to gemini surfactants with hydrophobic spacers is presented in Ref. 50. It introduces the following additions and modifications to the model outlined in Section II.B.

1. The hydrophobic free energy g_{hc} contains, apart from the double-tail contribution, a spacer contribution also. Only the spacer section which penetrates in the micellar hydrophobic core, s_{core}, is considered. This spacer section is taken simply as the difference between the total spacer length and the mean head–head distance, $s_{core} = s - a^{1/2}/b$. Because the three chains (two tails and spacer) are already in partial contact prior to aggregation, the hydrophobic energy gain per hydrocarbon group is taken to be smaller than in the case of a single-tail surfactant.

2. The interfacial term, $g_{\text{int}}(a)$, is modified to account for the part of the core–water interfacial area that is now occupied by the spacer. The chain length that participates in this shielding is proportional to $a^{1/2}$. This contribution is thus

$$\delta g_{\text{int}} \simeq (\gamma_2 - \gamma_1) a^{1/2} w \tag{20}$$

where γ_2 is the spacer–water interfacial tension and w is the spacer width. If the spacer is a polymethylene chain, then $\gamma_2 = \gamma_1$ and this correction vanishes.

3. When the spacer is short, it forces the two tails to be closer together than they would be if they belonged to two separate molecules. This packing constraint reduces the entropy of the tail chains. For a single-tail surfactant, the area close to the core-water surface sampled by tail groups is $a_{\text{tail}} \sim v/R$ (cf. Fig. 1), with a prefactor of order unity that varies with aggregate shape [23,50]. The proximity to a second tail due to the spacer reduces this available area per tail to $a_{\text{sp}} \sim (sb)^{2.}$ Thus, the contribution to the free energy can be estimated as

$$g_{\text{tail}} \simeq k_B T \ln\left(\frac{a_{\text{tail}}}{a_{\text{sp}}}\right) \simeq k_B T \ln\left(\frac{v}{Rb^2 s^2}\right) \tag{21}$$

4. Finally, the most difficult modification to handle is the electrostatic one. A short spacer forces the distance between two connected head groups to be shorter than that between two unconnected ones, resulting in a nonuniform charge distribution of pairs over the micellar surface (cf. Fig. 3). This problem is bypassed in Ref. 50 by introducing an empirical correction factor to g_{es}, which becomes equal to unity when the spacer is longer than the mean interhead distance.

This extended phenomenological model is applied in Ref. 50 to gemini surfactants with short hydrophobic spacers, using parameters known from regular single-tail and double-tail surfactants. The model yields cmc values for various tail lengths in good agreement with the measured ones. More important, it correctly accounts for the observed micelle shapes of *m-s-m* surfactants with small s (i.e., the crossover from cylinders to spheres as s is increased). Following the changes in the various free-energy contributions, one can identify the crossover mechanism as a competition between the elastic and packing contributions from the tails (favoring cylinders), and the electrostatic contribution (favoring spheres). Note, however, the various assumptions and approximations involved in these calculations. Although the electrostatic contribution to the free energy is found to be crucial for the self-assembly behavior, it is treated somewhat dubiously, as already admitted in Ref. 50.

2. Computer Simulations

The additional complexity introduced by the spacers makes analytical calculations very difficult. One is inclined, therefore, to resort to computer simulations in order to gain detailed information on the self-assembly of gemini surfactants.

The statistical–mechanical approach based on Monte Carlo (MC) simulations, as outlined in Section II.B, was extended to treat gemini surfactants [51,52]. The spin assignment to various groups and the corresponding energy function are the same as for regular, monomeric surfactants [see Eq. (14)]. The main modification is the connection of head groups in pairs via spacers (Fig. 5). Both hydrophobic spacers (spins $\sigma = -1$) and hydrophilic ones ($\sigma = +1$) were simulated. In addition, the role of spacer stiffness was checked by assigning an energy penalty for "kinks" in the spacer configuration.

This spin model reproduces a few important properties of gemini surfactants as observed in experiments, primarily the nonmonotonous dependence of the cmc on spacer length for hydrophobic spacers and the formation of

1	1	1	1	1	1	1	1	1	1
1	1	1	1	−1	−1	−1	2	1	1
1	1	2	−1	−1	1	1	0	1	1
1	1	0	1	1	1	1	−1	1	1
1	1	−1	1	1	1	1	−1	1	1
1	1	−1	1	1	1	1	−1	1	1
1	1	−1	−1	1	1	1	−1	1	1
1	1	1	−1	1	1	1	−1	1	1
1	1	1	1	1	1	1	1	1	1

FIG. 5 Schematic representation of a gemini surfactant molecule (gray) solubilized in water (white) in a lattice spin model. The spin scheme is similar to that of Fig. 2, except that the two hydrophilic head groups (spin +2) of each surfactant are linked by a spacer chain. The spacer is composed of spins −1 for hydrophobic spacers, as shown here, or +1 for hydrophilic spacers. In addition, a "kink" in the spacer chain such as the one shown here is assigned an energy penalty in order to mimic the role of spacer stiffness.

branched and entangled wormlike micelles in the case of short hydrophobic spacers (see Fig. 6). However, the MC simulations produce also some findings which are not in full accord with experiments. The cmc is found to *increase* with tail length, unlike the common experimental results (with the exception of Ref. 53). The mechanism for such a cmc increase with surfactant hydrophobicity is unclear. It is hard to simply attribute it to spacer–head repulsion because the increase is found to be insensitive to the "spin" associated with the head group. A similar issue appears in the cmc dependence for hydrophilic spacers, which is found to *decrease* with spacer length, in disagreement with the experimentally observed (and expected) increase [4]. The maximum in the cmc as a function of s is obtained for long hydrophobic spacers of about $s \simeq 12$ regardless of tail length, contrary to the experimental result of

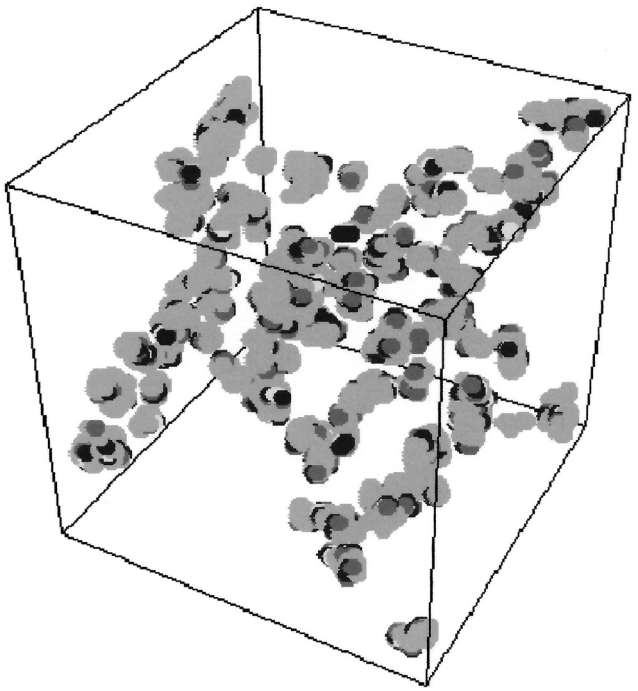

FIG. 6 Wormlike micelles formed in a MC simulation of the spin model. The gemini surfactant has 2 heads of 1 lattice site each, 2 neutral groups of 1 site each, 2 tails of 15 sites each, and a hydrophobic spacer of 2 sites. Different gray tones correspond to different surfactant groups. The water molecules are not shown for clarity. (Reprinted with permission from Ref. 51.)

only $s \simeq 5$ [6–8]. Surfactants with long ($s = 16$) hydrophobic spacers are found to form rodlike cylindrical micelles, whereas in experiments, they form bilayers [14]. Hence, the spin model investigated by MC simulations seems to capture part of the essential features of gemini surfactant self-assembly while missing others.

The bead–spring MD approach discussed in Section II.B was extended as well to treat gemini surfactants [36,37]. The only essential modification is the connection of head groups in pairs by spacer chains. Like the tail chains, the spacers are made of oillike particles connected to one another by harmonic springs, where only hydrophobic spacers were studied. These MD simulations are able to reproduce the micellar shapes formed by the *m-s-m* gemini surfactants–branched wormlike micelles and ring micelles—compared to the spherical morphology formed by the corresponding monomeric surfactants (see Fig. 7). A similar coarse-grained MD approach, along with a self-consistent-field calculation, were applied to the more complex glucitol amine gemini surfactants, which have flexible sugar side chains attached to the charged head groups [54]. The main finding is a transition from cylindrical micelles to bilayers upon increasing pH, in accord with experimental indications [55].

C. Phase Behavior

The spacer length has an unusual effect also on the phase behavior of systems containing *m-s-m* gemini surfactants. This fact has been mentioned already in Section I. For binary surfactant–water mixtures, the regions in the concentration-temperature phase diagrams, where single-phase hexagonal and lamellar phases are the stable state, become smaller as s increases, vanish for $s = 10$–12, and then are finite again for $s = 16$ [16]. In ternary water–oil–surfactant phase diagrams of the same surfactants, the size of the microemulsion (single-phase) region increases with s and then decreases, with a maximum at $s \simeq 10$ [17].

These observations can be rationalized in the light of the packing considerations discussed in Sections III.A and III.B [1]. As s increases from low values, the optimal area per molecule $a(s)$ increases and the packing parameter P of Eq. (6) decreases. Hence, surfactant packing into bilayers, which are the building blocks of the lamellar and hexagonal mesophases, becomes less and less favorable. As we have seen in the previous sections, this effect is maximal for $s = 10$–12, whereupon bilayers apparently can no longer be stabilized. When s increases further, a decreases, and bilayers can form again. This qualitative description agrees also with the experimental results for *m*-EO_x-m gemini surfactants. The observed monotonous increase in the phase-diagram region belonging to the isotropic micellar phase [56] is in

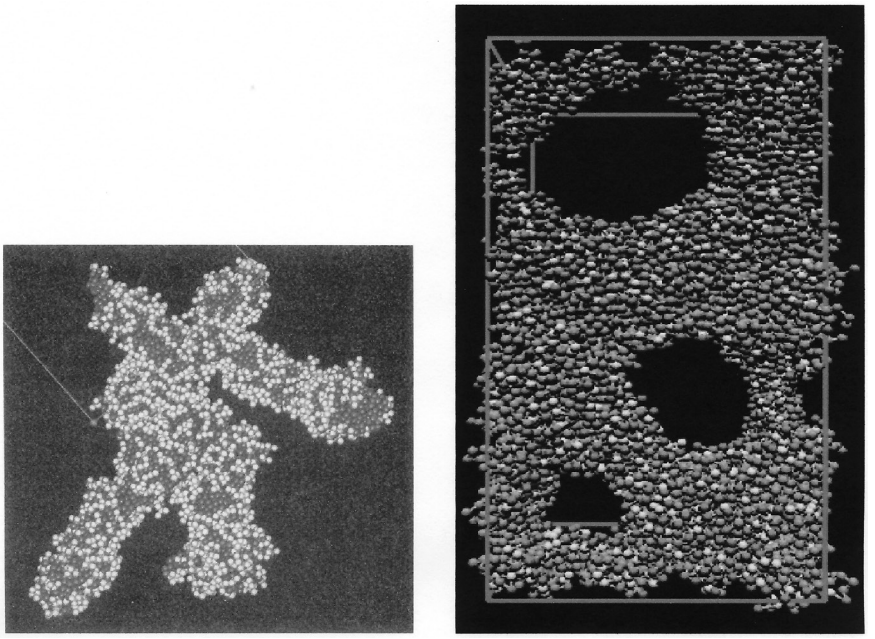

FIG. 7 Micelles formed in coarse-grained MD simulations of gemini surfactants. Left: branched wormlike micelle. The surfactant has two heads of three waterlike particles each, two tails of six oillike particles each, and a spacer of one oillike particle. Different gray tones correspond to different surfactant groups. The water molecules are not shown for clarity. (Reprinted with permission from Ref. 36. Copyright 1994 American Association for the Advancement of Science.) Right: ring micelles. The surfactant has two heads of one waterlike particle each, two tails of four oillike particles, and a spacer of two oillike particles. Different gray tones correspond to different surfactant groups. The water molecules are not shown for clarity. (Reprinted with permission from Ref. 37. Copyright 2002 American Chemical Society.)

accord with the moderate monotonous increase of $a(s)$ observed for these surfactants at the water–air interface [4].

In ternary oil-water–surfactant mixtures, as s increases and P decreases, the surfactant monolayers required for stabilizing a microemulsion can have a higher curvature. Hence, smaller oil domains can form and the microemulsion region in the phase diagram extends toward a higher surfactant concentration. This effect, too, should be maximal for $s = 10$–12, as observed in the experiment [17].

A theoretical study of gemini surfactant phase behavior, using MC simulations of a lattice model and a theory of mixture thermodynamics, is

presented in Ref. 57. Employing a simulation technique which, after equilibration, samples the composition of small regions in the entire lattice, the model is insensitive to long-ranged structures and is rather focused on the thermodynamics of phase coexistence. The study was restricted also to short hydrophilic spacers. Thus, the result cannot be compared with the above-mentioned experiments. The main finding is the suppression of the three-phase region (coexistence of water-rich, oil-rich, and surfactant-rich phases) upon introducing molecular rigidity.

IV. CONCLUSIONS AND OPEN QUESTIONS

The unusual self-assembly behavior of gemini surfactants poses challenging puzzles to theoretical investigations. We have reviewed the currently available models that attempt to address these puzzles, concentrating on surface properties, micellization, and phase behavior of gemini surfactant solutions. The overall impression emerging from the current state of the art is that, despite several successes, the theoretical understanding of gemini surfactants is fragmentary and lags behind the wealth of available experimental data.

As demonstrated in this review, current gemini surfactant models are based on previous theories of surfactant self-assembly, with the most essential modifications required due to the addition of the spacer chains. It seems that this route has been exhausted, and further progress will depend on detailed consideration of features distinguishing gemini surfactants from regular monomeric ones.

One of the distinct factors that stands out as a crucial ingredient is the spacer effect on lateral organization of the surfactant molecules in water-air monolayers and at aggregate surfaces. Linking the head groups in pairs has at least three different aspects as can be seen in Fig. 3. (1) The distribution of head groups on the surface becomes inhomogeneous, as linked head groups have a mutual distance different from that of unlinked ones. This should affect, for example, the surface charge distribution. (2) The spacers give the surfactant molecule an inplane orientation (i.e., the combined head group made of the two monomeric heads and spacer is asymmetric). Such a breakdown of isotropy, as is known from other systems, may lead to drastic effects on the overall behavior and may result in the formation of in-plane liquid-crystalline order. Nematic ordering due to elongated head groups was theoretically addressed in the case of bilayer membranes [58]. A recent work combining dichroism spectroscopy and atomistic MD simulations has revealed orientational ordering of gemini surfactants in cylindrical micelles [42]. More theoretical work is required to elucidate this issue. (3) The above two aspects apply as well to double-tail surfactants (e.g., phospholipids) with large, elongated head groups. What truly distinguishes gemini surfactants

from double-tailed surfactants is the fact that the spacer makes a soft link between the head groups. Containing at least several chemical bonds, it allows a degree of conformational flexibility to the entire molecule (e.g., with respect to the relative orientations of the two tails). This feature is probably what allows gemini surfactants to form such uncommon structures as branched micelles and ring micelles. In the MD simulations of Ref. 36, for example, the gemini surfactants residing in a branching junction of a wormlike micelle were found to have their two tails oriented in different directions. This property might also make gemini surfactants serve as cross-linkers of regular micelles [59]. Hence, it seems that our understanding of gemini surfactant self-assembly will be incomplete until we have a good account of the interplay among various lateral organizations of these molecules at surfaces.

Another important direction where there is substantial experimental information but almost no theory is the dynamics and rheology of gemini surfactant solutions. This aspect is particularly relevant to applications, as these solutions exhibit unusual and useful rheological properties such as shear thickening at low volume fractions [1]. Moreover, recently these properties have made micellar solutions of gemini surfactants a model system for studying nonequilibrium behaviors such as shear thickening and ultraslow relaxation [21]. We note that the dynamic issues and the issue of molecular organization mentioned earlier may be closely related. It has been argued recently that the distinct rheological behavior of wormlike micellar solutions (e.g., shear thickening) stems from the formation and interlinking of ring micelles [60].

We hope that this review and the posed open questions will motivate further theoretical studies of this class of fascinating and very useful self-assembling molecules.

ACKNOWLEDGMENTS

We are grateful to Raoul Zana for introducing us to the field of gemini surfactants and for numerous discussions and suggestions. We also benefited from discussions with Igal Szleifer. H.D. acknowledges support from the Israeli Council of Higher Education (Alon Fellowship). D.A. would like to acknowledge partial support from the Israel Science Foundation under grant No. 210/02 and the Alexander von Humboldt Foundation for a research award.

REFERENCES

1. Zana, R. J. Colloid Interf. Sci. 2002, *248*, 203–220.
2. Alami, E.; Beinert, G.; Marie, P.; Zana, R. Langmuir 1993, *9*, 1465–1467.

3. Perez, L.; Pinazo, A.; Rosen, MJ.; Infante, M.R. Langmuir 1998, *14*, 2307–2315.
4. Dreja, M.; Pyckhout-Hintzen, W.; Mays, H.; Tieke, B. Langmuir 1999, *15*, 391– 399.
5. Zhu, Y.P.; Masuyama, A.; Kobata, Y.; Nakatsuji, Y.; Okahara, M.; Rosen, M.J. J. Colloid Interf. Sci. 1993, *158*, 40–45.
6. Zana, R.; Berraou, M.; Rueff, R. Langmuir 1991, *7*, 1072–1075.
7. Devinsky, F.; Lacko, I.; Imam, T. Acta Fac. Pharm. 1990, *44*, 103.
8. De, S.; Aswal, VK.; Goyal, PS.; Bhattacharya, S. J. Phys. Chem. 1996, *100*, 11,664–11,671.
9. Zana, R. J. Colloid Interf. Sci. 2002, *252*, 259–261.
10. Grosmaire, L.; Chorro, M.; Chorro, C.; Partyka, S.; Zana, R. J. Colloid Interf. Sci. 2002, *246*, 175–181.
11. Israelachvili, J.; Mitchell, J.; Ninham, B.W. J. Chem. Soc. Faraday Trans. 2 1976, *72*, 1525–1568.
12. Israelachvili, JN. *Intermolecular and Surface Forces*, 2nd Ed.; Academic Press: San Diego, CA, 1991.
13. Zana, R.; Talmon, Y. Nature 1993, *362*, 228–230.
14. Danino, D.; Talmon, Y.; Zana, R. Langmuir 1995, *11*, 1448–1456.
15. Bernheim-Groswasser, A.; Zana, R.; Talmon, Y. J. Phys. Chem. B 2000, *104*, 4005–4009.
16. Alami, E.; Levy, H.; Zana, R.; Skoulios, A. Langmuir 1993, *9*, 940–944.
17. Dreja, M.; Gramberg, S.; Tieke, B. Chem. Commun. 1998, *13*, 1371–1372.
18. Kern, F.; Lequeux, F.; Zana, R.; Candau, SJ. Langmuir 1994, *10*, 1714–1723.
19. In, M.; Bec, V.; Aguerre-Chariol, O.; Zana, R. Langmuir 2000, *16*, 141–148.
20. Schmitt, V.; Schoseler, F.; Lequeux, F. Europhys. Lett. 1995, *30*, 31–36.
21. Oelschlaeger, C.L.; Waton, G.; Candau, S.J.; Cates, M.E. Langmuir 2002, *18*, 7265–7271.
22. Adamson, A.W.; Gast, A.P. *Physical Chemistry of Surfaces*, 6th Ed.; Wiley: New York, 1997.
23. Nagarajan, R.; Ruckenstein, E. Langmuir 1991, *7*, 2934–2969.
24. Tanford, C. *The Hydrophobic Effect*; Wiley: New York, 1980.
25. Evans, D.F.; Ninham, B.W. J. Phys. Chem. 1983, *87*, 5025–5032.
26. Widom, B. J. Chem. Phys. 1986, *84*, 6943–6954.
27. Larson, R.G.; Scriven, L.E.; Davis, H.T. J. Chem. Phys. 1985, *83*, 2411–2420.
28. Larson, R.G. J. Chem. Phys. 1992, *96*, 7904–7918.
29. Stauffer, D.; Jan, N.; Pandey, R.B. Physica A 1993, *198*, 401–409.
30. Stauffer, D.; Jan, N.; He, Y.; Pandey, R.B.; Marangoni, D.G.; Smith-Palmer, T. J. Chem. Phys. 1994, *100*, 6934–6942.
31. Jan, N.; Stauffer, D. J. Phys. I (France) 1994, *4*, 345–350.
32. Smit, B.; Hilbers, P.A.J.; Esselink, K.; Rupert, L.A.M.; van Os, N.M.; Schlijper, A.G. Nature 1990, *348*, 624–625.
33. Smit, B.; Esselink, K.; Hilbers, P.A.J.; Vanos, N.M.; Rupert, L.A.M.; Szleifer, I. Langmuir 1993, *9*, 9–11.
34. Palmer, B.J.; Liu, J. Langmuir 1996, *12*, 746–753.
35. Fodi, B.; Hentschke, R. Langmuir 2000, *16*, 1626–1633.

36. Karaborni, S.; Esselink, K.; Hilbers, P.A.J.; Smit, B.; Karthauser, J.; van Os, N.M.; Zana, R. Science 1994, *266*, 254–256.
37. Maiti, P.K.; Lansac, Y.; Glaser, M.A.; Clark, N.A. Langmuir 2002, *18*, 1908–1918.
38. Watanabe, K.; Ferrario, M.; Klein, M.L. J. Phys. Chem. 1988, *92*, 819–821.
39. Shelley, J.C.; Sprik, M.; Klein, M.L. Langmuir 1993, *9*, 916–926.
40. Mackerell, A.D. J. Phys. Chem. 1995, *99*, 1846–1855.
41. Maillet, J.B.; Lachet, V.; Coveney, P.V. Phys. Chem. Chem. Phys. 1999, *1*, 5277–5290.
42. Oda, R.; Laguerre, M.; Huc, I.; Desbat, B. Langmuir 2002, *18*, 9659–9667.
43. Gompper, G.; Schick, M. In *Phase Transitions Critical Phenomena*; Domb, C., Lebowitz, J.L., Eds; Academic Press: London, 1994.
44. In *Micelles, Membranes, Micromulsions, Monolayers*; Gelbart, W.M.; Ben-Shaul, A.; Roux, D.; Eds.; Springer-Verlag: New York, 1994.
45. Safran, S.A. *Statistical Thermodynamics of Surfaces, Interfaces, Membranes*; Addison-Wesley: New York, 1994.
46. Diamant, H.; Andelman, D. Langmuir 1994, *10*, 2910–2916.
47. Diamant, H.; Andelman, D. Langmuir 1995, *11*, 3605–3606.
48. Flory, P.J. *Statistical Mechanics of Chain Molecules*, 2nd Ed; Hanser: Cincinnati, OH, 1989.
49. Menger, F.M.; Wrenn, S. J. Phys. Chem. 1974, *78*, 1387–1390.
50. Camesano, T.A.; Nagarajan, R. Colloid Surfaces A 2000, *167*, 165–177.
51. Maiti, P.K.; Chowdhury, D. Europhys. Lett. 1998, *41*, 183–188.
52. Maiti, P.K.; Chowdhury, D. J. Chem. Phys. 1998, *109*, 5126–5133.
53. Menger, F.M.; Littau, C.A. J. Am. Chem. Soc. 1993, *115*, 10083–10090.
54. van Eijk, M.C.P.; Bergsma, M.; Marrink, S.J. Eur. Phys. J. E 2002, *7*, 317–324.
55. Fielden, M.L.; Perrin, C.; Kremer, A.; Bergsma, M.; Stuart, M.C.; Camilleri, P.; Engberts, J.B.F.N. Eur. J. Biochem. 2001, *268*, 1269–1279.
56. Dreja, M.; Tieke, B. Langmuir 1998, *14*, 800–807.
57. Layn, K.M.; Debenedetti, P.G.; Prud'homme, R.K. J. Chem. Phys. 1998, *109*, 5651–5658.
58. Fournier, J.B.; Galatola, P. J. Phys. II (France) 1997, *7*, 1509–1520.
59. Maiti, P.K.; Kremer, K. Langmuir 2000, *16*, 3784–3790.
60. Cates, M.E.; Candau, S.J. Europhys. Lett. 2001, *55*, 887–893.